Delay controls chimera relay synchronization in multiplex networks

Jakub Sawicki, Iryna Omelchenko, Anna Zakharova, and Eckehard Schöll*
Institut für Theoretische Physik, Technische Universität Berlin, Hardenbergstraße 36, 10623 Berlin, Germany

(Received 3 August 2018; revised manuscript received 12 December 2018; published 28 December 2018)

We study remote (or relay) synchronization in multilayer networks between parts of one layer and their counterparts in a second layer, where these two layers are not directly connected. A simple realization of such a system is a triplex network where a relay layer in the middle, which is generally not synchronized, acts as a transmitter between two outer layers. We establish time delay in the interlayer coupling as a powerful tool to control various partial synchronization patterns, in particular chimera states, i.e., complex patterns of coexisting coherent and incoherent domains. We demonstrate that the three-layer structure of the network allows for synchronization of the coherent domains of chimera states in the first layer with their counterparts in the third layer, whereas the incoherent domains either remain desynchronized or synchronized. By varying the topology of the relay layer, we study its influence on the remote synchronization in the outer layers. As model dynamics we use the paradigmatic FitzHugh-Nagumo system.

DOI: 10.1103/PhysRevE.98.062224

I. INTRODUCTION

Complex networks are ubiquitous in nature and technology, and the analysis of their nonlinear dynamics and synchronization properties gives insight into diverse real-world systems [1–5]. Recently, research has focused on multilayer networks, which provide a description of systems interconnected through different types of links. The interplay of intralayer interaction with interlayer coupling opens up a plethora of phenomena in different fields; see, e.g., [6–9]. A prominent example of such structures is social networks, which can be described as groups of people with different patterns of contacts or interactions between them [10]. Other relevant applications are communication, supply, and transportation networks, for instance power grids, subway networks, or air-traffic networks [11]. In biology, multilayer networks represent, for instance, neurons in different areas of the brain or neurons connected either by a chemical link or by an electrical synapsis [12,13]. A special case of multilayer networks is multiplex topologies, where each layer contains the same set of nodes, and only pairwise connections between corresponding nodes from neighboring layers exist [14–19].

Relay (or remote) synchronization between layers which are not directly connected is an intriguing phenomenon, which extends previously known relay synchronization between single systems, e.g., chaotic lasers [20]. The synchronization of network layers, which interact via an intermediate (relay) layer, has recently provoked much interest [21]. The simplest realization of such a system is a triplex network where a relay layer in the middle acts as a transmitter between the two outer layers. Network symmetries play an essential role in remote synchronization, where pairs of nodes synchronize despite their large distances on the network graph [22–25].

In neuroscience various scenarios have been uncovered where specific brain areas act as a functional relay between other brain regions, having a strong influence on signal propagation, brain functionality, and dysfunctions [26,27]. For instance, the relay cells of the thalamus serve both as the primary relay of sensory information from the periphery to the cortex and as an interactive hub of communication between cortical areas [28–31]. They enable visual processing [32] and rapid coordination of spatially segregated cortical computations important for cognitive flexibility, cognitive control, and its perturbation in disease states [33]. Parahippocampal regions can be considered as relay stations, which actively gate impulse traffic between neocortex and hippocampus, with strong implications for the propagation of neural activity [34]. The hippocampus also acts as a relay in the cortico-cortical theta synchronization [35,36]; signal transmission between cortical and subcortical brain regions is involved in a wide range of brain functions [37]. Especially, partial relay synchronization plays an important role in experiments with mice [36], where just a part of the hippocampal relay exhibits phase-lag synchronization with the two cortical regions, which between themselves exhibit partial zero-lag synchronization.

In networks of isolated layers different types of dynamics have been observed, depending on the nature of the individual nodes and the topology within the layer [38,39]. Besides complete synchronization, cluster synchronization, or desynchronized chaotic dynamics, more complex spatio-temporal patterns can be observed. Chimera states are prominent example of such patterns: they combine spatially coexisting domains of coherence and incoherence [40–45]. Initially found in nonlocally coupled rings of identical oscillators, chimera states have recently been observed in a variety of network models with different topologies [46–52] and realized experimentally [53–60]. Chimera states are reminiscent of partially synchronized patterns in brain dynamics [61], such as unihemispheric sleep [62,63] and epileptic seizure [64–68] or

*Corresponding author: schoell@physik.tu-berlin.de

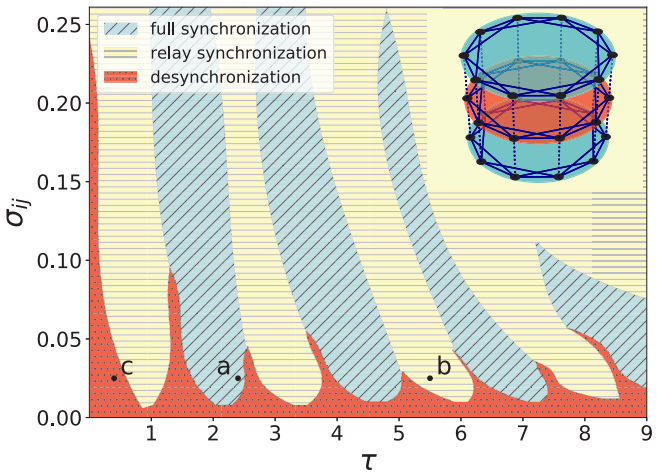

FIG. 1. Relay synchronization tongues in the parameter plane of interlayer coupling strength $\sigma_{ij} \equiv \sigma_{12} = \sigma_{23}$ and interlayer coupling delay $\tau > 0$. Interlayer relay synchronization (horizontally hatched yellow region) occurs between regions of full interlayer synchronization (diagonally hatched blue region) and desynchronized interlayer dynamics (dotted dark red regions). Black dots a, b, and c denote parameter values of the synchronization scenarios shown in Fig. 2. Random initial conditions were used for all numerical simulations. Parameters are $\varepsilon = 0.05$, $a = 0.5$, $\sigma_i = 0.2$, $R_i = 170$ for $i = 1, 2, 3$, $\phi = \frac{\pi}{2} - 0.1$, $N = 500$. The inset shows a schematic triplex network. The middle layer $i = 2$ (dark red) acts as relay layer between the outer layers $i = 1, 3$ (blue).

even perceptual organization [69] and behavioral sensitization [70,71].

It is the purpose of the present paper to extend the notion of relay synchronization from completely synchronized states to partial synchronization patterns in the individual layers and study various scenarios of synchronization of chimera states in a three-layer multiplex network of FitzHugh-Nagumo oscillators. This model is a paradigmatic system widely used in neuroscience and electrical engineering. Our analysis shows that the three-layer structure of the network gives rise to partial or full synchronization of chimera states in the outer layers via the relay layer. Our focus is on the control of the chimera synchronization patterns by time delay in the interlayer coupling. Varying the coupling range, i.e., the topology, of the relay layer allows one to establish its effect on the remote synchronization in the outer layers. Our results might have widespread applications, including encrypted communication and neuronal dynamics.

II. MODEL

The inset of Fig. 1 shows the configuration of a multiplex network with three layers (triplex). Each layer consists of a ring of N identical FitzHugh-Nagumo (FHN) oscillators with nonlocal (intralayer) coupling of coupling range R_i in layer $i = 1, 2, 3$, i.e., each oscillator is coupled with R_i neighbors to the left and to the right. Layers 1 and 3 (light blue) are coupled through the intermediate layer 2 (dark red), so that the middle layer acts as a relay between the two outer layers, but there is no interlayer coupling between layers 1 and 3. The dynamical equations are given by

$$\dot{\mathbf{x}}_k^i(t) = \mathbf{F}\big(\mathbf{x}_k^i(t)\big) + \frac{\sigma_i}{2R_i} \sum_{l=k-R_i}^{k+R_i} \mathbf{H}\big[\mathbf{x}_l^i(t) - \mathbf{x}_k^i(t)\big] + \sum_{j=1}^{3} \sigma_{ij} \mathbf{H}\big[\mathbf{x}_k^j(t-\tau) - \mathbf{x}_k^i(t)\big], \tag{1}$$

where $\mathbf{x}_k^i = (u, v)^T \in \mathbb{R}^2$, $i \in \{1, \ldots, 3\}$, $k \in \{1, \ldots, N\}$, with all indices modulo N, denotes the set of activator (u) and inhibitor (v) variables, and the dynamics of each individual oscillator is governed by

$$\mathbf{F}(\mathbf{x}) = \begin{pmatrix} \varepsilon^{-1}\big(u - \frac{u^3}{3} - v\big) \\ u + a \end{pmatrix}, \tag{2}$$

where $\varepsilon > 0$ describes the timescale separation between fast activator and slow inhibitor, fixed at $\varepsilon = 0.05$ throughout this paper. Depending on the threshold parameter a, the single FHN elements exhibit either oscillatory ($|a| < 1$) or excitable ($|a| > 1$) behavior. Here we choose the oscillatory regime ($a = 0.5$). The parameter σ_i denotes the intralayer coupling strength, while σ_{ij} is the interlayer coupling strength. We use time delay τ only in the interlayer coupling, since in real-world systems the transfer of information between two different layers is often slower than within one layer. In order to ensure constant row sum we choose the interlayer coupling as $\sigma_{12} = \sigma_{32}$, $\sigma_{21} = \sigma_{23} = \sigma_{32}/2$, and $\sigma_{11} = \sigma_{13} = \sigma_{22} = \sigma_{31} = \sigma_{33} = 0$. The interaction is realized through diffusive coupling with coupling matrix

$$\mathbf{H} = \begin{pmatrix} \varepsilon^{-1}\cos\phi & \varepsilon^{-1}\sin\phi \\ -\sin\phi & \cos\phi \end{pmatrix} \tag{3}$$

and coupling phase $\phi = \frac{\pi}{2} - 0.1$. This coupling scheme, which consists predominantly of activator-inhibitor cross-coupling, is similar to a phase lag of approximately $\pi/2$ in the Kuramoto phase oscillator model and has been chosen such that chimera states are most likely to occur [72].

III. RESULTS

Generally, a time delay τ in the coupling often leads to spatially traveling patterns as shown in [73]. The same effect is observed for our multiplex network in case of delayed interlayer coupling. Consequently, it is not possible to extract any information from measures calculated over a long time, e.g., the mean phase velocity profile and the local interlayer synchronization error E_k^{ij} introduced below, where each node has a fixed index k independent of the dynamics in the system. By detrending the data we can avoid this problem: After each time step in the numerical simulation we re-index the nodes k in such a way that $k' = (k + c)$, where c is given by the center of the largest domain of the ring where for all k's of that domain $\|\mathbf{x}_k(t) - \mathbf{x}_{k+1}(t)\| < \theta$ with a threshold θ chosen as $\theta = 0.25$ (see Appendix A). By doing so we shift the node indices such that we follow the largest coherent domain on the ring if it moves.

For a single-layer network it is known that for appropriate coupling strength σ_i and coupling range R_i complex patterns of spatially coexisting coherent and incoherent dynamics, i.e., chimera states, can occur and they may be centered at different spatial locations depending on the initial conditions [72]. On the other hand, it has been shown recently [21] that in multiplex networks one can achieve synchronization of either neighboring or remote layers. However, the synchronization of complex spatio-temporal patterns like chimera states in multiplex networks is still largely unresolved. Here we establish the possibility to control partial synchronization patterns even of remote layers, in particular chimera states, by tuning the interlayer coupling strength σ_{ij} and delay τ. Varying these two parameters allows for an overall control of the dynamical regimes in the network. An appropriate measure for instantaneous synchronization between two layers i, j is the global interlayer synchronization error E^{ij}, defined by

$$E^{ij} = \lim_{T\to\infty} \frac{1}{NT} \int_0^T \sum_{k=1}^{N} \left\| \mathbf{x}_k^j(t) - \mathbf{x}_k^i(t) \right\| dt, \tag{4}$$

where $\|\cdot\|$ stands for the Euclidean norm, and the normalization by N allows for better comparison of networks of different size (see Appendices B and C). First we consider three identical layers. Regarding the interlayer synchronization three dynamical regimes are conceivable:

(1) *full interlayer synchronization* where synchronization exists between all three layers ($E^{12} = E^{13} = 0$);

(2) *relay interlayer synchronization* where synchronization exists just between the two outer layers ($E^{12} \neq 0$ and $E^{13} = 0$);

(3) *interlayer desynchronization* ($E^{12} \neq E^{13} \neq 0$).

Numerical simulations in Fig. 1 show that we can observe all scenarios depending on the parameters and the initial conditions (here, random initial conditions). When the layers are coupled weakly, they tend to behave independently (red dotted region): Each layer exhibits a chimera state but there is no synchronization between the layers. With increasing delay $\tau > 0$ (the case $\tau = 0$ must be treated separately; see Appendix B) we observe a sequence of tongue-like regions in the parameter plane (τ, σ_{ij}): Full interlayer synchronization (blue regions with diagonal stripes) alternating with relay interlayer synchronization (yellow regions with horizontal stripes). Exemplary snapshots of the dynamics in these synchronized regions are shown in Figs. 2(a) and 2(b) (left column). We can observe full in-phase synchronization of all three layers for values of τ close to integer multiples of the period of the uncoupled system $T = 2.3$, and relay interlayer synchronization with antiphase synchronization between the outer layers and the relay layer for half-integer multiples. Analytical calculations show that the period T decreases with increasing σ_{ij} (see Appendix D). Therefore, due to the resonance condition of τ with respect to the intrinsic period T, the tongues are shifted to the left with increasing coupling strength σ_{ij}. The same effect occurs when τ equals higher multiples of the intrinsic period, where the tongues are shifted more strongly to the left and decrease in size, which is a general feature of resonance tongues in delay systems [74,75]. To study the

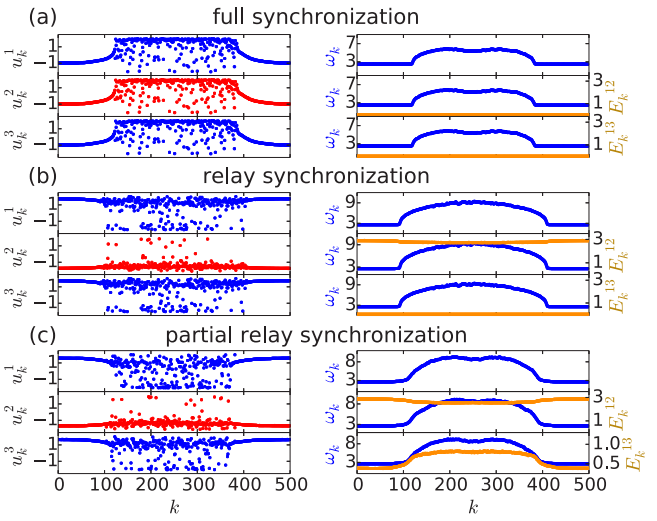

FIG. 2. Dynamics of the three layers for different values of delay time τ, marked by black dots a, b, c in Fig. 1. (a) Full interlayer synchronization for $\tau = 2.4$. (b) Relay interlayer synchronization for $\tau = 5.5$. (c) Partial relay interlayer synchronization between the outer layers for $\tau = 0.4$. The left column shows snapshots of variables u_k^i for all three layers $i = 1, 2, 3$ [relay layer: red (light gray), outer layers: blue (dark gray)], whereas the right column shows the corresponding mean phase velocity profiles ω_k [dark blue (dark gray)] for each layer and interlayer synchronization error E_k^{ij} [orange (light gray)]. Interlayer coupling is given by $\sigma_{ij} = 0.025$, other parameters are as in Fig. 1.

synchronization of chimera patterns between the layers in more detail, we use the local interlayer synchronization error in dependence on each node k:

$$E_k^{ij} = \lim_{T\to\infty} \frac{1}{T} \int_0^T \left\| \mathbf{x}_k^j(t) - \mathbf{x}_k^i(t) \right\| dt. \tag{5}$$

This measure is useful in detecting those nodes which are synchronized between two layers, especially in the (red dotted) region of desynchronization in Fig. 1. Exemplary dynamics inside this region are given in Fig. 2(c): We can see the arc-shaped profiles for both mean phase velocity ω_k and local interlayer synchronization error E_k^{13}. This means that the coherent parts of the chimera states are synchronized between the outer layer, whereas the incoherent parts are not. This kind of synchronization may be called *partial relay interlayer synchronization* or *double chimera*, since it denotes coherence-incoherence behavior within the layers and between the layers. It cannot be detected by the global interlayer synchronization error $E^{ij} \neq 0$, but the node-dependent local measure E_k^{ij} gives us the possibility to distinguish this type of synchronization. In Fig. 2 (right column) E_k^{ij} is plotted (light orange) together with the mean phase velocity profile ω_k (dark blue) for a typical chimera state. The mean phase velocity of the oscillators is calculated as $\omega_k = 2\pi S_k/\Delta T$, $k = 1, \ldots, N$, where S_k denotes the number of complete rotations realized by the kth oscillator during the time ΔT. Throughout the paper we use $\Delta T = 10\,000$.

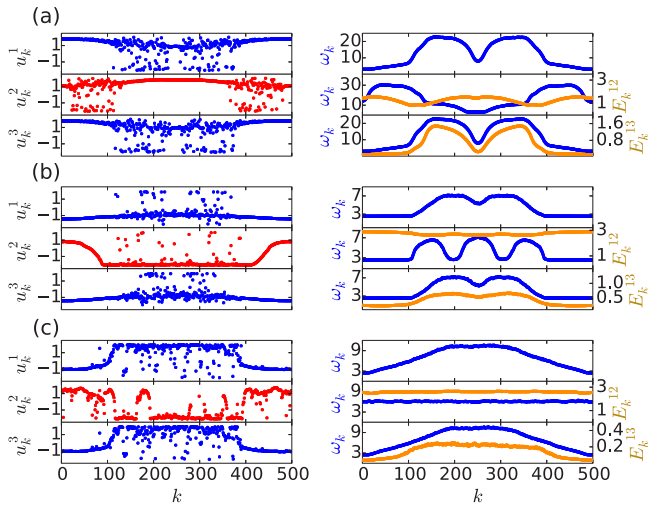

FIG. 3. Partial relay interlayer synchronization between the outer layers: snapshots of variables u_k^i (left column) for layers $i = 1, 2, 3$ [relay layer: red (light gray); outer layers: blue (dark gray)], and mean phase velocity profiles ω_k [dark blue (dark gray)] and interlayer synchronization error E_k^{ij} [orange (light gray)] in the right column. (a) $R_1 = R_2 = R_3 = 170$, $\tau = 1.3$, $\sigma_{ij} = 0.025$; (b) $R_1 = R_3 = 150$, $R_2 = 130$, $\tau = 0.4$, $\sigma_{ij} = 0.015$; (c) $R_1 = R_3 = 150$, $R_2 = 10$, $\tau = 0.8$, $\sigma_{ij} = 0.01$. Other parameters are as in Fig. 1.

In our simulations we observe different intriguing types of partial relay interlayer synchronization; for instance, Fig. 3(a) depicts an example ($\tau = 1.3$) where the relay layer exhibits antisynchronization of chimera patterns: the coherent domain of the relay layer (red, middle panel) spatially coincides with the incoherent domains of the outer layers.

In addition, to demonstrate the robustness of our findings, we vary the topology of the relay layer compared to the outer layers by changing its coupling range. Fig. 3(b) shows partial relay interlayer synchronization for the case of small mismatch of the coupling range in the relay and outer layers ($R_1 = R_3 = 150$, $R_2 = 130$). The middle layer exhibits a chimera state with three incoherent domains, in contrast to two in the outer layers, and the coherent domains in the relay layer and the outer layers are in antiphase. The local synchronization error E_k^{13} between the two outer layers is nonzero in the incoherent domains and vanishes for the coherent domains, as a signature of partial relay synchronization.

Moreover, for large mismatch of the coupling ranges in the relay and outer layers [see Fig. 3(c) where $R_1 = R_3 = 150$ and $R_2 = 10$], the relay layer is characterized by chaotic dynamics. This strongly chaotic dynamics of the relay naturally affects the chimera states in the outer layers, so that their mean phase velocity profiles (dark blue) are smeared out despite of detrending. Nevertheless, the coherent domains of the chimera states are synchronized between the outer layers, whereas the incoherent parts are not, as shown in the snapshots and the plot of E_k^{13}. Thus, the relay synchronization mechanism turns out to be robust with respect to changes of the relay layer topology. Preliminary studies show that this holds also for a mismatch of the excitation parameter a between the layers (see Appendix E).

IV. CONCLUSIONS

There is some analogy between the full relay synchronization in a three-layer network and in a three-node network of delay-coupled lasers [20]; see also [76], where the similarity between an active and a passive relay is elaborated and intuitively explained by two delayed feedback loops which describe the passive relay (semitransparent mirror). Taking into account the quotient network behind the three-layer network, one intuitively expects the outer layers to behave the same way because of the underlying symmetry. Extending the three-node network to the much more complex phenomenon of partial relay synchronization of chimera states was a motivation for the present study. A simple three-node relay network cannot reproduce this phenomenon.

Here we have shown that multilayer networks allow for intriguing remote synchronization scenarios. Relay synchronization of chimeras between the outer layers of a multiplex network is an example of such a scenario, where distant layers of the network synchronize in spite of the absence of direct connections between them. We have analyzed relay synchronization in a three-layer network of FitzHugh-Nagumo oscillators, with nonlocal coupling topologies within the layers, and have extended the notion of relay synchronization to chimera states.

Chimera patterns can be observed in each network layer; they are usually strongly dependent on the initial conditions, and it is not possible to predict which part of the network will form coherent domains. By relay synchronization we can fix the location to the same position as in the other outer layer. Varying the strength of the coupling between the network layers, we observe various scenarios of synchronization of chimera states, either in all three layers or only in the two outer layers. As measures we employ the global and local interlayer synchronization errors and mean phase velocity profiles of the oscillators.

Time delay in the interlayer coupling, which is ubiquitous in real-world systems, has been identified as a powerful tool for control of the patterns: It allows for observation of novel synchronization scenarios where the coherent domains of chimera states in the outer layers are synchronized, while the incoherent domains are not. The relay layer remains desynchronized and exhibits various multichimera patterns, or even chaotic dynamics. Furthermore, partial relay synchronization of chimeras states in the two outer layers has been realized in the form of intriguing double chimeras, where the coherent domains in both layers are synchronized, while the incoherent ones are not. By choosing an appropriate value for the time delay we can switch between the different synchronization scenarios.

Control of chimera patterns can also be effected by changing the topology in the intermediate layer. By varying the coupling range we find that even strongly diluted relay layers allow for remote synchronization of chimeras in the outer layers, while the relay layer stays in the chaotic regime.

We propose that our findings may be useful in the study of novel concepts for encrypted and secure communication, where relay synchronization of complex spatio-temporal patterns, for instance chimera states, can be employed. Since the dynamics of the intermediate (relay) layer is not synchronized,

it does not transmit information to someone listening in. While relay synchronization of single chaotic lasers has been extensively investigated in the context of encrypted communication [20], here we have extended and generalized the concept of relay synchronization to multilayer networks, which exhibit much more complex dynamics. As brain networks are often described as multilayer structures, our results may also help in elucidating complex scenarios of information processing in neural networks. Recent research in neuroscience indicates that many parts of the brain, e.g., thalamus, interneurons, and hippocampus, act as relays that connect two different regions [30,32,33,77]. In particular, we have shown that specifically the hitherto unexplained experiments on imperfect synchronization in the mice brain [36] might be explained by our novel scenarios of partial relay interlayer synchronization (see Appendix F). Our analysis of relay synchronization scenarios in multiplex networks could thus help us to understand dynamical patterns in the mammalian or human brain.

ACKNOWLEDGMENT

This work was supported by Deutsche Forschungsgemeinschaft in the framework of Collaborative Research Center SFB 910.

APPENDIX A: DETRENDING

Introducing a time delay τ in the coupling term often leads to traveling patterns as shown, e.g., in [73]. Additionally, chimera states are associated with complex dynamics sensitively depending on initial conditions, and it is difficult to obtain general dependencies of the velocity of the traveling pattern on the delay or the coupling strength. For our multiplex network [see Eq. (A1)], in case of delayed interlayer coupling we observe the same effect [see Fig. 4(c)]:

$$\dot{\mathbf{x}}_k^i(t) = \mathbf{F}\big(\mathbf{x}_k^i(t)\big) + \frac{\sigma_i}{2R_i}\sum_{l=k-R_i}^{k+R_i}\mathbf{H}\big[\mathbf{x}_l^i(t) - \mathbf{x}_k^i(t)\big] + \sum_{j=1}^{3}\sigma_{ij}\mathbf{H}\big[\mathbf{x}_k^j(t-\tau) - \mathbf{x}_k^i(t)\big]. \tag{A1}$$

Consequently, it is not possible to achieve any information from measures calculated over a long time, e.g., the mean-phase velocity profile and local interlayer synchronization error E_k^{ij} [see Fig. 4(a)]. By detrending the data we can avoid this problem: After each time-step in the numerical simulation we re-index the nodes k in such a way that $k' = (k+c)|_N$, where $|$ stands for the modulo operator and c is given by the center of the largest domain of the ring where for all k's of that domain $\|x_k(t) - x_{k+1}(t)\| < \theta$. As the threshold parameter θ we choose $\theta = 0.25$. The effect of that method is shown in Fig. 4: Without detrending [Fig. 4(a)] no information can be achieved from the mean phase velocity profile and the local/global interlayer synchronization error; applying detrending leads to well pronounced arc-shaped profiles of both measures [Fig. 4(b)]. In Fig. 4 E_k^{13} is plotted (light red) together with the mean phase velocity $\omega(k)$ (dark blue) for a typical chimera state. Since the chimera patterns are traveling

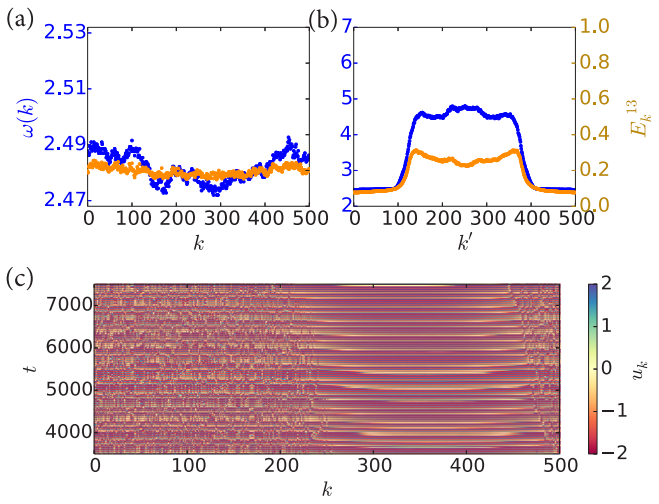

FIG. 4. Detrending of simulation data. By re-indexing the nodes for each numerical step we can detect chimera states which shift temporally along the ring, for instance, induced by delayed coupling. The upper left panel (a) shows raw simulation data for the mean phase velocity ω_k [dark blue (dark gray)] and local interlayer synchronization error E_k^{13} [orange (light gray)], whereas the upper right panel (b) shows the same data after detrending, i.e., re-indexing. A typical arc-shaped profile is recognizable now. The lower panel (c) shows a space-time plot of the variable u_k for a traveling chimera inside a layer. Simulations were performed for $\sigma_i = 0.2$, $\sigma_{ij} = 0.01$, $R_1 = R_3 = 150$, $R_2 = 110$, and $\tau = 0.7$. Other parameters are as in Fig. 2.

along the ring, averaging over a time window does not lead to a clear chimera-type profile (a). However, after re-indexing the nodes after each time-step such that the coherent domain remains at a fixed spatial position ("detrending") we can see the arc-shaped profiles for both mean phase velocity $\omega(k)$ and local interlayer synchronization error E_k^{13} (b).

APPENDIX B: UNDELAYED CASE

In the case of an undelayed interlayer coupling ($\tau = 0$) full interlayer synchronization and relay interlayer synchronization are possible. Numerical simulations in Fig. 5 show that we can observe two synchronization mechanisms depending on the initial conditions (here, random initial conditions) combined with chimera states: Already for small interlayer coupling strength $\sigma_{ij} > 0.01$ relay interlayer synchronization is possible. By increasing σ_{ij} the middle layer also tends to synchronize with the outer layers. At a critical value of the coupling strength ($\sigma_{ij} = 0.12$) this relay synchronization mechanism cannot be observed anymore, and the full interlayer synchronization mechanism remains. This mechanism exists over the whole range of σ_{ij}: By increasing σ_{ij} the three layers tend to full interlayer synchronization at $\sigma_{ij} = 0.24$. For $\sigma_{ij} < 0.01$ no synchronization can be observed in the case of random initial conditions. Nevertheless, in the case of $\tau = 0$, full interlayer synchronization can always be achieved for any value of σ_{ij} by choosing full interlayer synchronization as initial conditions. In that case the interlayer coupling term in Eq. (A1) vanishes due to the diffusive coupling form.

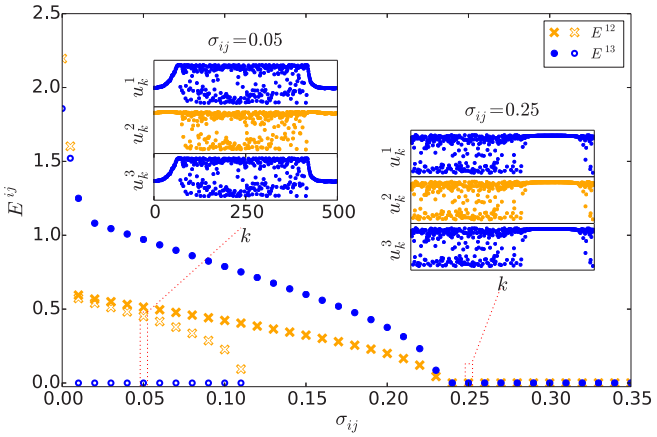

FIG. 5. Two synchronization mechanisms in a triplex network with identical layers [Eq. (A1)] and undelayed interlayer coupling ($\tau = 0$). The main plot shows the global interlayer synchronization error E^{ij} between the first and second layers (yellow crosses, E^{12}) and between the outer layers (blue circles, E^{13}) versus the interlayer coupling $\sigma_{ij} = \sigma_{12} = \sigma_{23}$. The filled markers correspond to the full synchronization mechanism, whereas the unfilled ones to the relay synchronization mechanism. Already for small interlayer couplings ($0.01 < \sigma_{ij} < 0.12$) we can observe either relay interlayer synchronization or the transition to full interlayer synchronization, whereas for greater values of the coupling strength ($\sigma_{ij} > 0.12$) just the latter one is observable. The insets show snapshots of variables u_k^i for all three layers i on top of each other for two different interlayer coupling strengths $\sigma_{ij} = 0.05$ and 0.25, respectively. These values correspond to the two synchronization mechanisms, respectively. For all simulations random initial conditions are used. Parameters are chosen as $\varepsilon = 0.05$, $a = 0.5$, $\sigma_i = 0.05$, $N = 500$, $R_i = 170$, $\phi = \frac{\pi}{2} - 0.1$, and $i = 1, 2, 3$.

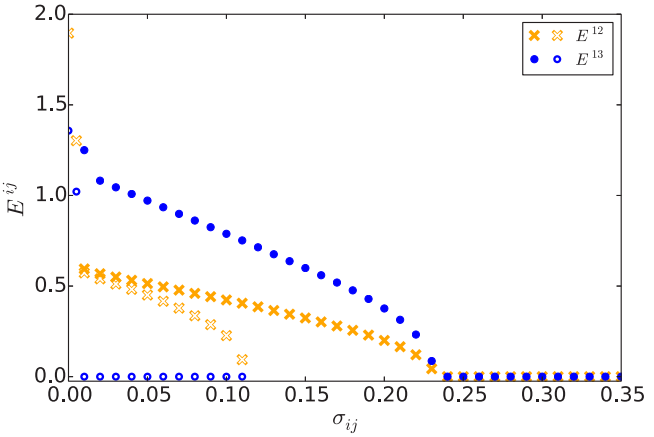

FIG. 6. Two synchronization mechanisms in a triplex network of size $N = 1000$. The plot shows the global interlayer synchronization error E^{ij} between the first and second layers (yellow crosses, E^{12}) and between the outer layers (blue circles, E^{13}) versus the interlayer coupling $\sigma_{ij} = \sigma_{12} = \sigma_{23}$. The filled markers correspond to the full synchronization mechanism, whereas the unfilled ones to the relay synchronization mechanism. For all simulations random initial conditions are used. The coupling range is given by $R_i = 340$, other parameters are as in Fig. 5.

APPENDIX C: NETWORK SIZE DEPENDENCE

An appropriate measure for synchronization between two layers i, j is the global interlayer synchronization error E^{ij}, defined by

$$E^{ij} = \lim_{T\to\infty} \frac{1}{NT} \int_0^T \sum_{k=1}^{N} \left\| \mathbf{x}_k^j(t) - \mathbf{x}_k^i(t) \right\| dt, \qquad \text{(C1)}$$

where $\|\cdot\|$ stands for the Euclidean norm, and the normalization by N allows for better comparison of networks of different size. The maximum value of E^{ij} does not depend on the node number N, as we can see in Fig. 6: Compared to Fig. 5 the network size was doubled but the values of the synchronization errors E^{ij} remain the same.

APPENDIX D: ESTIMATE OF PERIOD

In many delay systems one expects resonance effects if the delay is an integer or half-integer multiple of the period of the uncoupled system [74,75,78]. For full interlayer synchronization the undelayed part of the coupling term in the ith layer is the most important part in case of incoherent dynamics and can be rewritten as follows, neglecting $\cos\phi \ll 1$ and setting $\sin\phi \approx 1$:

$$\begin{aligned} \varepsilon \dot{u} &= u - \frac{u^3}{3} - (1 + \sigma_i + \sigma_{ij})v, \\ \dot{v} &= (1 + \sigma_i + \sigma_{ij})u + a. \end{aligned} \qquad \text{(D1)}$$

Similar to Brandstetter [79] we employ an analytic approximation for the period of the oscillation defined by Eq. (D1). We consider slow motion on the falling branches of the u nullcline given by $(1 + \sigma_i + \sigma_{ij})v = u - \frac{u^3}{3}$ and hence $(1 + \sigma_i + \sigma_{ij})\dot{v} = \dot{u}(1 - u^2)$, which gives

$$\dot{u} = \frac{(1 + \sigma_i + \sigma_{ij})^2 u + (1 + \sigma_i + \sigma_{ij})a}{1 - u^2}. \qquad \text{(D2)}$$

It is possible to integrate this equation analytically from $\pm u_+$ to $\pm u_-$, which are approximately the limits of the slow parts of the u nullcline, given by $u_+ = 2$ and $u_- = 1$. With this we obtain a rough approximation of the intrinsic period $T(\sigma_{ij})$ of the coupled system, neglecting the fast parts of the trajectory $u(t)$:

$$\begin{aligned} T(\sigma_{ij}) \propto\ & (1 + \sigma_i + \sigma_{ij})^{-2} \\ & \times \left[u_+^2 - u_-^2 + \left(1 - \left(\frac{a}{1 + \sigma_i + \sigma_{ij}} \right)^2 \right) \ln \right. \\ & \left. \times \frac{a^2 - (1 + \sigma_i + \sigma_{ij})^2 u_-^2}{a^2 - (1 + \sigma_i + \sigma_{ij})^2 u_+^2} \right]. \end{aligned} \qquad \text{(D3)}$$

The period T decreases with increasing σ_{ij}. Therefore, due to the resonance condition of τ with respect to the intrinsic period T, the synchronization tongues are shifted to the left with increasing coupling strength σ_{ij}.

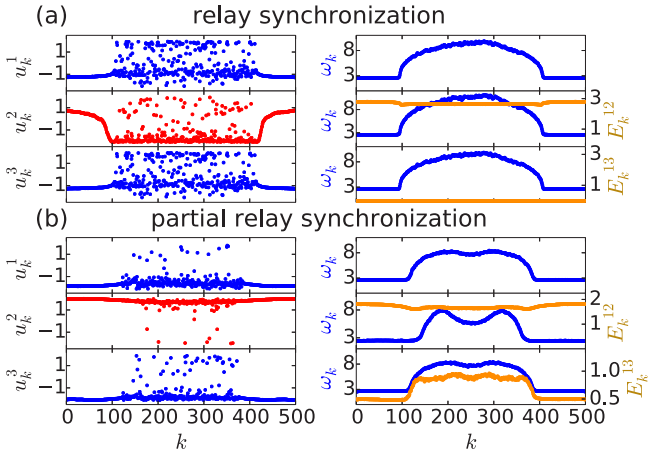

FIG. 7. Dynamics of the three layers for mismatched excitation parameters $a_1 = a_3 = 0.5$ and $a_2 = 0.6$. (a) Relay interlayer synchronization for $\tau = 5.5$. (b) Partial relay interlayer synchronization between the outer layers for $\tau = 0.4$. The left column shows snapshots of variables u_k^i for all three layers $i = 1, 2, 3$ [relay layer: red (light gray); outer layers: blue (dark gray)], whereas the right column shows the corresponding mean phase velocity profiles ω_k [dark blue (dark gray)] for each layer and interlayer synchronization error E_k^{ij} [orange (light gray)]. Interlayer coupling is given by $\sigma_{ij} = 0.025$, intralayer coupling is given by $\sigma_i = 0.2$, other parameters are as in Fig. 5.

APPENDIX E: MISMATCHED EXCITATION PARAMETERS

In general there exist several parameters which can render the relay layer different from the outer layers. So far we have focused on the topology R_i to make the relay layer different from the outer layers. Another possibility is to vary the dynamics of the nodes, so the dynamics of each individual oscillator is governed by

$$\mathbf{F}(\mathbf{x}) = \begin{pmatrix} \varepsilon^{-1}\left(u - \frac{u^3}{3} - v\right) \\ u + a_i \end{pmatrix}, \tag{E1}$$

where each layer i has a specific threshold parameter a_i. In Fig. 7 we show that the phenomenon of (partial) relay synchronization can also be observed in the case where there is a mismatch between the excitation parameters in the outer layers and the relay layer ($a_1 = a_3 \neq a_2$).

APPENDIX F: COMPARISON WITH EXPERIMENTAL RESULTS

Recently it has been asserted that several regions in the brain, e.g., the thalamus and hippocampus, act as a relay element between two distant regions in the brain [33]. In [36] the authors suggest that synchronization between two neocortical regions in the brain is likely to be mediated by the hippocampus as a relay layer. They report that two distant neuronal populations, namely the frontal (F) and visual (V) cortexes, are able to synchronize at almost zero time lag if a third element, the hippocampus (H), acts as a relay between them [see Fig. 8(a)]. This relay symmetrically redistributes its incoming signals between the two other regions. Experiments suggest that zero-lag neuronal synchrony occurs in the

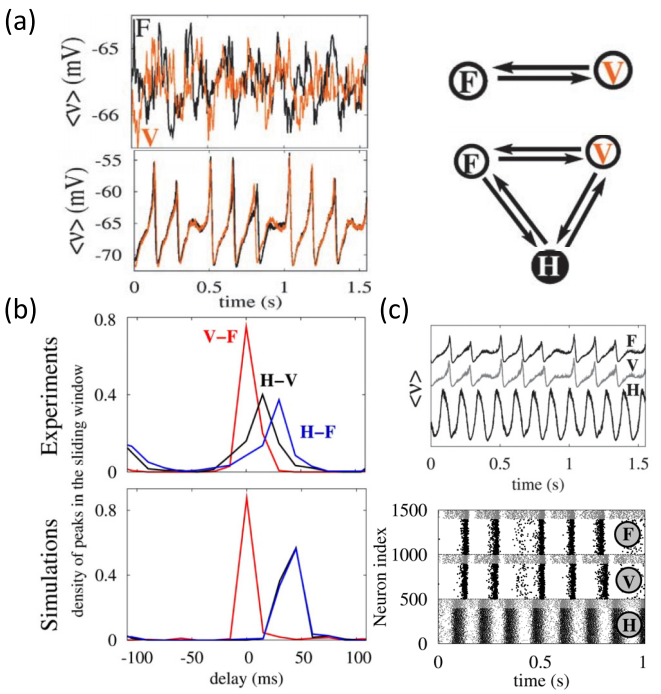

FIG. 8. Comparison with experimental results [36]. (a) Measured time series (left column) of average voltage v in mV of two cortical regions, frontal (F, black) and visual (V, light orange). The upper panel shows desynchronization and corresponds to the case of a two-layer network (see right column), whereas the lower panel shows zero-lag synchronization and corresponds to a three-layer network, where the two cortical regions are additionally connected with the hippocampal relay (H). (b) Spatio-temporal synchronization obtained from the experimental (upper panel) and numerical data (lower panel). Plotted is the density of spikes in the sliding window (300 ms) of filtered time series cross-correlation between the three layers F, V, H. Experimental data correspond to a mouse. (c) Modeling of neuronal dynamics. Lower panel: space-time plot of 500 neurons in each layer. Upper panel: ensemble average voltage of the three layers vs time in s. All panels are from [36].

brain in the presence of large axonal conduction delays [35]. Moreover, it has been shown in experiments with mice that the relay element itself is synchronized with a constant phase lag [see Fig. 8(b)]. To simulate these experiments the authors in [36] suggest a network model, where the two different regions F, V of size $N = 500$ are not only connected via the relay element H, but are also mutually coupled. In our model of a triplex network (same size as [36]) we show that by introducing delay in the interlayer connections one is able to achieve relay synchronization, where no direct connection between the outer layers is necessary, which is more in line with the real structure of the human brain. Furthermore, in our simulations [e.g., Fig. 7, or Figs. 2(b), 2(c), and 3] the relay layer is synchronized with a constant phase lag similar to the experiments in [36]. Finally, with our scenario of double chimera (partial relay interlayer synchronization) we are able to propose an explanation of the imperfect synchronization shown in Figs. 8(b) and 8(c): For special delay times just a part of the outer layers is synchronized, whereas some parts stay desynchronized.

[1] A. Pikovsky, M. G. Rosenblum, and J. Kurths, *Synchronization: A Universal Concept in Nonlinear Sciences* (Cambridge University Press, Cambridge, 2001).
[2] S. H. Strogatz, Nature (London) **410**, 268 (2001).
[3] R. Albert and A. L. Barabási, Rev. Mod. Phys. **74**, 47 (2002).
[4] M. E. J. Newman, SIAM Rev. **45**, 167 (2003).
[5] S. Boccaletti, A. N. Pisarchik, C. I. del Genio, and A. Amann, *Synchronization: From Coupled Systems to Complex Networks* (Cambridge University Press, Cambridge, 2018).
[6] S. Boccaletti, G. Bianconi, R. Criado, C. I. del Genio, J. Gómez-Gardeñes, M. Romance, I. Sendiña Nadal, Z. Wang, and M. Zanin, Phys. Rep. **544**, 1 (2014).
[7] M. De Domenico, A. Solé-Ribalta, E. Cozzo, M. Kivelä, Y. Moreno, M. A. Porter, S. Gómez, and A. Arenas, Phys. Rev. X **3**, 041022 (2013).
[8] M. De Domenico, V. Nicosia, A. Arenas, and V. Latora, Nat. Commun. **6**, 6864 (2015).
[9] M. Kivelä, A. Arenas, M. Barthélemy, J. P. Gleeson, Y. Moreno, and M. A. Porter, J. Complex Networks **2**, 203 (2014).
[10] M. Girvan and M. E. J. Newman, Proc. Natl. Acad. Sci. USA **99**, 7821 (2002).
[11] A. Cardillo, M. Zanin, J. Gòmez Gardeñes, M. Romance, A. Garcia del Amo, and S. Boccaletti, Eur. Phys. J. Spec. Top. **215**, 23 (2013).
[12] B. Bentley, R. Branicky, C. L. Barnes, Y. L. Chew, E. Yemini, E. T. Bullmore, P. E. Vétes, and W. R. Schafer, PLoS Comput. Biol. **12**, 1 (2016).
[13] F. Battiston, V. Nicosia, M. Chavez, and V. Latora, Chaos **27**, 047404 (2017).
[14] X. Zhang, S. Boccaletti, S. Guan, and Z. Liu, Phys. Rev. Lett. **114**, 038701 (2015).
[15] V. A. Maksimenko, V. V. Makarov, B. K. Bera, D. Ghosh, S. K. Dana, M. V. Goremyko, N. S. Frolov, A. A. Koronovskii, and A. E. Hramov, Phys. Rev. E **94**, 052205 (2016).
[16] S. Jalan and A. Singh, Europhys. Lett. **113**, 30002 (2016).
[17] S. Ghosh and S. Jalan, Int. J. Bifurc. Chaos **26**, 1650120 (2016).
[18] I. Leyva, R. Sevilla-Escoboza, I. Sendiña-Nadal, R. Gutiérrez, J. M. Buldú, and S. Boccaletti, Sci. Rep. **7**, 45475 (2017).
[19] R. G. Andrzejak, G. Ruzzene, and I. Malvestio, Chaos **27**, 053114 (2017).
[20] M. C. Soriano, J. García-Ojalvo, C. R. Mirasso, and I. Fischer, Rev. Mod. Phys. **85**, 421 (2013).
[21] I. Leyva, I. Sendiña-Nadal, R. Sevilla-Escoboza, V. P. Vera-Avila, P. Chholak, and S. Boccaletti, Sci. Rep. **8**, 8629 (2018).
[22] V. Nicosia, M. Valencia, M. Chavez, A. Díaz-Guilera, and V. Latora, Phys. Rev. Lett. **110**, 174102 (2013).
[23] L. V. Gambuzza, A. Cardillo, A. Fiasconaro, L. Fortuna, J. Gómez-Gardeñes, and M. Frasca, Chaos **23**, 043103 (2013).
[24] L. Zhang, A. E. Motter, and T. Nishikawa, Phys. Rev. Lett. **118**, 174102 (2017).
[25] Y. Zhang, T. Nishikawa, and A. E. Motter, Phys. Rev. E **95**, 062215 (2017).
[26] P. Roelfsema, A. Engel, P. König, and W. Singer, Nature (London) **385**, 157 (1997).
[27] D. S. Soteropoulos and S. N. Baker, J. Neurophysiol. **95**, 1194 (2006).
[28] S. M. Sherman, Nat. Neurosci. **19**, 533 (2016).
[29] P. A. Rhodes and R. Llinas, J. Physiol. **565**, 765 (2005).
[30] R. W. Guillery and S. M. Sherman, Neuron **33**, 163 (2002).
[31] L. L. Gollo, C. R. Mirasso, and A. E. P. Villa, NeuroImage **52**, 947 (2010).
[32] X. Wang, V. Vaingankar, C. S. Sanchez, F. T. Sommer, and J. A. Hirsch, Nat. Neurosci. **14**, 224 (2011).
[33] M. M. Halassa and S. Kastner, Nat. Neurosci. **20**, 1669 (2017).
[34] M. de Curtis and D. Paré, Prog. Neurobiol. **74**, 101 (2004).
[35] I. Fischer, R. Vicente, J. M. Buldú, M. Peil, C. R. Mirasso, M. C. Torrent, and J. García-Ojalvo, Phys. Rev. Lett. **97**, 123902 (2006).
[36] L. L. Gollo, C. R. Mirasso, M. Atienza, M. Crespo-Garcia, and J. L. Cantero, PLoS ONE **6**, e17756 (2011).
[37] J. A. Prasad and Y. Chudasama, J. Neurosci. **33**, 8494 (2013).
[38] S. Amari, Biol. Cybern. **27**, 77 (1977).
[39] A. Compte, N. Brunel, P. S. Goldman-Rakic, and X. J. Wang, Cereb. Cortex **10**, 910 (2000).
[40] Y. Kuramoto and D. Battogtokh, Nonlinear Phenom. Complex Syst. **5**, 380 (2002).
[41] D. M. Abrams and S. H. Strogatz, Phys. Rev. Lett. **93**, 174102 (2004).
[42] S.-i. Shima and Y. Kuramoto, Phys. Rev. E **69**, 036213 (2004).
[43] A. E. Motter, Nat. Phys. **6**, 164 (2010).
[44] M. J. Panaggio and D. M. Abrams, Nonlinearity **28**, R67 (2015).
[45] E. Schöll, Eur. Phys. J. Spec. Top. **225**, 891 (2016).
[46] A. Buscarino, M. Frasca, L. V. Gambuzza, and P. Hövel, Phys. Rev. E **91**, 022817 (2015).
[47] T. Banerjee, P. S. Dutta, A. Zakharova, and E. Schöll, Phys. Rev. E **94**, 032206 (2016).
[48] S. Ghosh, A. Kumar, A. Zakharova, and S. Jalan, Europhys. Lett. **115**, 60005 (2016).
[49] S. Majhi, M. Perc, and D. Ghosh, Chaos **27**, 073109 (2017).
[50] D. V. Kasatkin, S. Yanchuk, E. Schöll, and V. I. Nekorkin, Phys. Rev. E **96**, 062211 (2017).
[51] A. Bukh, E. Rybalova, N. Semenova, G. Strelkova, and V. Anishchenko, Chaos **27**, 111102 (2017).
[52] A. V. Bukh, G. I. Strelkova, and V. S. Anishchenko, arXiv:1802.02771.
[53] A. M. Hagerstrom, T. E. Murphy, R. Roy, P. Hövel, I. Omelchenko, and E. Schöll, Nat. Phys. **8**, 658 (2012).
[54] M. R. Tinsley, S. Nkomo, and K. Showalter, Nat. Phys. **8**, 662 (2012).
[55] E. A. Martens, S. Thutupalli, A. Fourriere, and O. Hallatschek, Proc. Natl. Acad. Sci. USA **110**, 10563 (2013).
[56] L. Larger, B. Penkovsky, and Y. Maistrenko, Phys. Rev. Lett. **111**, 054103 (2013).
[57] L. V. Gambuzza, A. Buscarino, S. Chessari, L. Fortuna, R. Meucci, and M. Frasca, Phys. Rev. E **90**, 032905 (2014).
[58] M. Wickramasinghe and I. Z. Kiss, PLoS ONE **8**, e80586 (2013).
[59] L. Schmidt, K. Schönleber, K. Krischer, and V. García-Morales, Chaos **24**, 013102 (2014).
[60] D. P. Rosin, D. Rontani, N. D. Haynes, E. Schöll, and D. J. Gauthier, Phys. Rev. E **90**, 030902(R) (2014).
[61] M. S. Santos, J. D. Szezech, F. S. Borges, K. C. Iarosz, I. L. Caldas, A. M. Batista, R. L. Viana, and J. Kurths, Chaos Solitons Fractals **101**, 86 (2017)
[62] N. C. Rattenborg, C. J. Amlaner, and S. L. Lima, Neurosci. Biobehav. Rev. **24**, 817 (2000).
[63] N. C. Rattenborg, B. Voirin, S. M. Cruz, R. Tisdale, G. Dell'Omo, H. P. Lipp, M. Wikelski, and A. L. Vyssotski, Nat. Commun. **7**, 12468 (2016).

[64] P. Jiruska, M. de Curtis, J. G. R. Jefferys, C. A. Schevon, S. J. Schiff, and K. Schindler, J. Physiol. **591**, 787 (2013).
[65] V. K. Jirsa, W. C. Stacey, P. P. Quilichini, A. I. Ivanov, and C. Bernard, Brain **137**, 2210 (2014).
[66] A. Rothkegel and K. Lehnertz, New J. Phys. **16**, 055006 (2014).
[67] R. G. Andrzejak, C. Rummel, F. Mormann, and K. Schindler, Sci. Rep. **6**, 23000 (2016).
[68] T. Chouzouris, I. Omelchenko, A. Zakharova, J. Hlinka, P. Jiruska, and E. Schöll, Chaos **28**, 045112 (2018).
[69] A. R. Nikolaev, S. Gepshtein, P. Gong, and C. van Leeuwen, Cereb. Cortex **20**, 365 (2010).
[70] S. Ahn and L. L. Rubchinsky, Chaos **23**, 013138 (2013).
[71] S. Ahn, L. L. Rubchinsky, and C. C. Lapish, Cereb. Cortex **24**, 2553 (2014).
[72] I. Omelchenko, O. E. Omel'chenko, P. Hövel, and E. Schöll, Phys. Rev. Lett. **110**, 224101 (2013).
[73] J. Sawicki, I. Omelchenko, A. Zakharova, and E. Schöll, Eur. Phys. J. Spec. Top. **226**, 1883 (2017).
[74] P. Hövel and E. Schöll, Phys. Rev. E **72**, 046203 (2005).
[75] S. Yanchuk, M. Wolfrum, P. Hövel, and E. Schöll, Phys. Rev. E **74**, 026201 (2006).
[76] V. Flunkert, O. D'Huys, J. Danckaert, I. Fischer, and E. Schöll, Phys. Rev. E **79**, 065201(R) (2009).
[77] S. D. Vann and A. J. D. Nelson, in *The Connected Hippocampus*, edited by S. O'Mara and M. Tsanov, Progress in Brain Research, Vol. 219 (Elsevier, Amsterdam, 2015), pp. 163–185.
[78] S. Yanchuk and P. Perlikowski, Phys. Rev. E **79**, 046221 (2009).
[79] S. A. Brandstetter, M. A. Dahlem, and E. Schöll, Philos. Trans. R. Soc. A **368**, 391 (2010).